MIMO Assisted Networks Relying on Intelligent Reflective Surfaces: A Stochastic Geometry Based Analysis

Tianwei Hou, *Member, IEEE,* Yuanwei Liu, *Senior Member, IEEE,* Zhengyu Song, Xin Sun, Yue Chen, *Senior Member, IEEE,* and Lajos Hanzo, *Fellow, IEEE*

***Abstract*—Intelligent reflective surfaces (IRSs) are invoked for improving both the spectral efficiency (SE) and energy efficiency (EE). Specifically, an IRS-aided multiple-input multiple-output network is considered, where the performance of randomly roaming users is analyzed by utilizing stochastic geometry tools. As such, to distinguish the superposed signals at each user, the passive beamforming weight at the IRSs and detection weight vectors at the users are jointly designed. As a benefit, by adopting a zero-forcing-based design, the intra-cell interference imposed by the IRS can be suppressed. In order to evaluate the performance of the proposed network, we first derive the approximated channel statistics in the high signal-to-noise-ratio (SNR) regime. Then, we derive the closed-form expressions both for the outage probability and for the ergodic rate of users. Both the high-SNR slopes of ergodic rate and the diversity orders of outage probability are derived for gleaning further insights. The network's SE and EE are also derived. Our numerical results are provided to confirm that: i) the high-SNR slope of the proposed network is one; ii) the SE and EE can be significantly enhanced by increasing the number of IRS elements.**

***Index Terms*—Intelligent reflective surfaces (IRS), multiple-input multiple-output, passive beamforming, stochastic geometry.**

TABLE I: LIST OF ACRONYMS

Binomial point process	BPP
Base station	BS
Channel state information	CSI
Downlink	DL
Energy efficiency	EE
Fifth generation	5G
Intelligent reflective surface	IRS
Line-of-sight	LoS
Millimeter wave	mmWave
Multiple-input Single-output	MISO
Multiple-input multiple-output	MIMO
Non-Line-of-sight	NLoS
Outage probability	OP
Probability density function	PDF
Signal-to-interference-plus-noise-ratio	SINR
Signal-to-noise-ratio	SNR
Spectral efficiency	SE
Stochastic geometry	SG

I. Introduction

In next-generation networks, many sophisticated wireless technologies have been proposed, such as massive multiple-input multiple-output (MIMO) schemes and intelligent reflective surfaces (IRSs). According to the fifth generation (5G) new radio standard, upon reaching out beyond 6GHz, the coverage area is significantly reduced [1], [2]. Since high-frequency signals are sensitive to blockage effects [3] of trees and buildings, the cost-effective technique of IRS-aided networks has been developed [4], [5], which can be integrated into the present infrastructures [6], [7]. An IRS-aided system relies on many reflective elements, each of which is able to adjust the phase shifts and possibly the amplitude of the incident signals. By aligning the signals reflected by the IRS elements, the received signal of both the base station (BS) and of the users can be constructively or destructively superimposed by appropriately adjusting the global channel state information (CSI) [8]–[11]. For convenience, the main acronyms in this article are listed in Table I.

Because of the revolutionary concept of IRS networks [12], many potential applications were proposed [13]–[15], with special emphasis on their physical layer security [16], cell edge enhancement [17] and IRS-aided simultaneous wireless information and power transfer [18]. Previous research illustrates that when the number of IRS elements is high enough, IRS networks are able to perform better than relay-aided networks [19]. Naturally, the BS-user link quality is critical. Hence in fading environments, IRSs may substantially enhance the received signals at the desired users or mitigate the interference [20]. Taking into account the effects of Rayleigh fading, the bit error ratio was evaluated in [21]. There is likely to be a line-of-sight (LoS) link between the BS and IRSs. Therefore, the ergodic rates were estimated in [22], where Rician fading environments were considered. The product

L. Hanzo would like to acknowledge the financial support of the Engineering and Physical Sciences Research Council projects EP/P034284/1 and EP/P003990/1 (COALESCE) as well as of the European Research Council's Advanced Fellow Grant QuantCom (Grant No. 789028). This paper is also supported by the National Natural Science Foundation of China under Grant 61901027. (Corresponding authors: Zhengyu Song and Lajos Hanzo.)

T. Hou, Z. Song and X. Sun are with the School of Electronic and Information Engineering, Beijing Jiaotong University, Beijing 100044, China (email: twhou@bjtu.edu.cn, songzy@bjtu.edu.cn, xsun@bjtu.edu.cn).

Y. Liu and Yue Chen are with School of Electronic Engineering and Computer Science, Queen Mary University of London, London E1 4NS, U.K. (e-mail: yuanwei.liu@qmul.ac.uk, yue.chen@qmul.ac.uk).

L. Hanzo is with University of Southampton, Southampton, U.K. (email:lh@ecs.soton.ac.uk).

of two cascaded fading channels was considered in [23], and the resultant probability density functions (PDF) were derived. The asymptotic transmission rate of IRS networks was evaluated in [24], where the impact of IRSs on the channel hardening was considered in Rician fading channels. Moreover, it is proved that IRS-aided non-orthogonal multiple access (NOMA) network performance better than orthogonal multiple access (OMA) networks [25], where the transmit power is optimized. Then, the passive beamforming at the IRSs is designed for the user with best channel gain in [26]. An IRS-aided multi-user network was proposed in [27], where multiple IRS arrays are simultaneously deployed for multiple users. However, since the IRS elements are produced by multiple diodes, the phase shifts of IRS elements are discrete in practice for an IRS-aided network [28]–[31]. In [32], an IRS-aided network for finite-resolution phase shifters was investigated, where the signal-to-interference-plus-noise-ratio (SINR) was optimized. In [33], [34], the authors proposed the associated energy consumption model, and then optimized the energy efficiency (EE) of the proposed networks. Then the power efficiency was optimized in a Multiple-input Single-output (MISO)-aided non-orthogonal multiple access network, and the proposed solution outperformed the classic zero-forcing-based active beamforming [35]. By contrast, due to the obstacles, the direct link between the BS and users is not always available [36]. Hence, the users located in coverage-holes can be served by IRSs. The blockage effect in the IRS-aided millimeter wave (mmWave) networks was considered in [37], where the signals were enhanced both for static and moving blockages. Since IRSs are passive infrastructure elements, the channel estimation of the BS-IRS-user links becomes a challenging issue [38]–[40]. The channel model of IRS-aided MIMO networks was evaluated in [41], where both the LoS BS-IRS and the NLos IRS-user links, as well as the NLoS BS-user links were considered. In order to better illustrate the channel model in practice, the distance, azimuth and elevation angles were considered in a 3-dimensional channel model [42], and the channel statistics were evaluated.

However, there is a paucity of literature quantifying the impact of user-locations on the attainable performance. Stochastic geometry (SG) constitutes an efficient mathematical tool for capturing the topological randomness of networks [43], [44]. The users were assumed to be randomly located according to a binomial point process (BPP) in [45], and the impact of location randomness in cellular networks was evaluated in [46]. The analytical results indicated that the system performance trends were not gravely affected by shadowing. As a further development, the authors of [11] quantified the probability that a randomly distributed object is coated with an IRS. Then, the blockages was modeled by a Boolean process for modeling the effect of deploying IRSs in cellular networks [47], and the ratio of blind-spots to adequate coverage areas was derived. The active and passive beamforming were indeed jointly designed in [48], where the desired signals and interferences were evaluated, but the associated closed-form expression remaind an open issue. The Poisson cluster process was considered in [49], and the angle of reflection was constrained by the angle of incidence. Therefore, the randomly distributed users and BSs were located at the same side of the RIS, which is an unrealistic simplifying assumption. The active beamforming at the BS and the detection vector at the users have to be re-considered. Hence, by taking into account the user-positions using SG, which is the objective of this treatise in order to conceive a practical IRS network.

A. Motivations and Contributions

On the one hand, the previous contributions [17], [20]–[22], [24], [31], [32], [34] have mainly been focussed on IRS-aided MISO networks, where only a single antenna is employed by the users. On the other hand, there is a lack of literature on the impact of the locations of multiple users. Motivated by the potential benefits of the IRS-aided networks, in this article we will provide the downlink (DL) analysis of a MIMO-IRS framework by using tools from SG. The proposed MIMO-IRS network has to solve three additional issues: i) Having multiple antennas and multiple IRS elements impose interference on the users; ii) LoS fading environments between the BS and IRSs has to be considered; iii) The passive beamforming technique we used at the multiple IRS elements also has to be reconsidered. In this article, the active beamforming weights employed at the BS combined with appropriately chosen detection vectors at the users perform well both in IRS and non-IRS scenarios. Table II boldly and explicitly contrasts our contributions to the literature, and the objective of the proposed model.

Against the above background, our contributions can be summarized as follows:

- An IRS-aided network is proposed, where SG is invoked for modelling the location randomness. By applying a zero-forcing-based design, the detection vector of the users combined with passive beamforming at the IRSs are conceived. Our novel contributions are boldly and explicitly contrasted to the literature in Table II. The outage probabilities, ergodic rates, spectral efficiencies (SEs), and EEs are characterized for evaluating the benefits of the proposed design.
- Explicitly, we first derive the exact distribution of the channel statistics in the high-signal-to-noise-ratio (high-SNR) regime by deriving the Laplace transform of the PDF. Then, we derive closed-form expressions of the outage probability (OP) for the proposed MIMO-IRS network. Both analytical and asymptotic results are derived. Furthermore, the associated diversity orders are obtained based on the OP developed. The results confirm that the diversity order of the proposed network mainly depends on the distribution of the fading between the BS and IRSs.
- We then derive the approximated distribution of the channel statistics. The closed-form expressions of the ergodic rate are derived, along with the associated high-SNR slopes. The close agreement between the approximated and simulation results confirms the accuracy of our low-complexity analytical method.
- The simulation results indicate that: 1) the spatial gain enhances the OP and ergodic rate; 2) the distribution of the fading of the IRS-user links only slightly impacts

TABLE II: Contrasting our contributions to the literature, and the objective of the proposed model.

	[4]	[5]	[19]	[23]	[34]	[41]	[42]	[48]	Proposed Model
IRS-aided network	✓	✓	✓	✓	✓	✓	✓	✓	✓
HD relaying under AF protocol					✓				✓
HD relaying under DF protocol	✓				✓				✓
Approximated distribution						✓	✓	✓	✓
Exact distribution				✓					✓
Path loss modeling					✓		✓	✓	✓
IRS positioning		✓							✓
Energy model			✓						✓
Stochastic geometry								✓	✓

TABLE III:
TABLE OF NOTATIONS

α	Path loss exponent.
R	The radius of the disc.
R_m	The target rate of user m.
t_1	Fading parameter between the BS and IRSs.
t_2	Fading parameter between the IRSs and users.
M	The number of antennas at the BS.
M	The number of users.
K	The number of antennas at users.
L	The amount number of IRSs.
$\mathbf{G}$	The channel matrix between the BS and IRSs.
$\mathbf{H}_m$	The channel matrix between the IRSs and user m.
$\mathbf{\Phi}$	The effective matrix of IRSs.

the network performance; 3) both the spectral efficiency (SE) and EE are significantly improved by increasing the number of IRS elements.

B. Organization and Notations

In Section II, our MIMO-IRS network is discussed. In Section III, the analytical results are evaluated to quantify the performance attained. Our numerical results in Section IV verify the accuracy of our analysis, which is followed by our conclusions in Section V. Table III lists some of the critical notations used in this article. $\mathbf{H}^{\mathrm{T}}$, $\mathbf{H}^{\mathrm{H}}$, $rank(\mathbf{H})$ and $tr(\mathbf{H})$ denote the transpose, conjugate transpose, rank and trace of the matrix $\mathbf{H}$. $\mathbb{P}(\cdot)$ and $\mathbb{E}(\cdot)$ denote the probability and expectation, respectively. The distribution of a random variable with mean x and covariance k is denoted by $\mathcal{RV}(x,k)$; and $\sim$ stands for 'distributed as'. $\Gamma(\cdot)$ represents the Gamma function, ${}_2F_2(\cdot,\cdot;\cdot,\cdot;\cdot)$ denotes the generalized hypergeometric series [50, eq. (9.141)], $\Gamma(\cdot,\cdot)$ is the Gamma distribution, $\gamma(\cdot,\cdot)$ represents the lower incomplete Gamma function, and $G(\cdot)$ denotes the Meijer-G function [50].

II. System Model

In the proposed IRS-aided MIMO networks, M transmitter antennas (TAs) and K receiver antennas (RAs) are used at a BS and users, respectively. Note that L IRS elements are co-located on an IRS array mounted on the same building positioned at the center of the disc, where L IRS elements simultaneously serve M users.[1] By appropriately controlling the phase shifts and amplitude coefficients of the IRS elements, the electromagnetic signal can be beneficially manipulated. Fig. 1 demonstrates the system model of the proposed IRS-aided network. Note that the inter-cell interference significantly affects the network's performance. However, the consideration of a multi-cell setup is beyond the scope of this treatise.

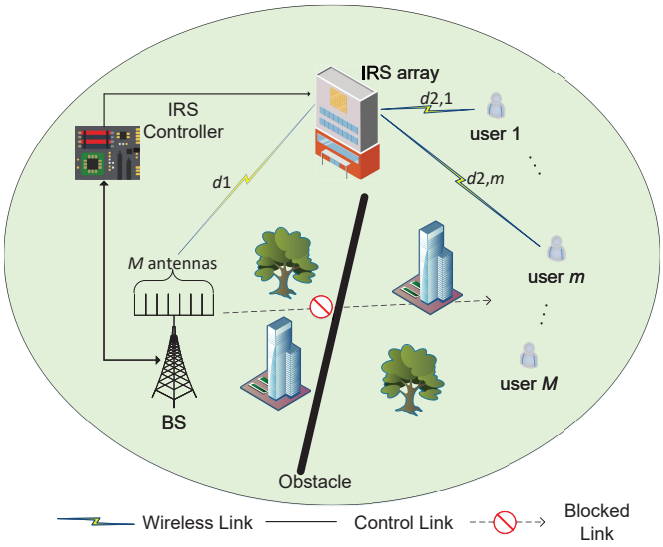

Fig. 1: Illustration of a typical IRS assisted wireless transmission model.

A. System Description

Since both the BS and IRSs are infrastructure elements, their locations are fixed. It is assumed that the distances between the BS and IRS array and that between the IRS array and user m are denoted by d_1 and $d_{2,m}$, respectively, where $d_{2,m}$ is a random value. In practice, the distances d_1 and $d_{2,m}$ are usually higher than 1 meter for simplifying the

[1]Since stochastic geometry tools were invoked, and based on the insights gleaned from [51], the object at the origin can be flexibly selected.

analytical results, where the parameter r_0 avoids encountering a singularity, when the distance is small [52]. Generally speaking, r_0 is set to 1 meter. Since the horizontal distance of the BS-IRS and IRS-user links is much higher than the vertical distance and the length of the IRS array, the height and the length of the IRS array is ignored. The M users are randomly distributed on a disc $\mathcal{R}^2$ having the radius R according to a BPP, where the direct BS-user transmission links are blocked by potential objects, i.e. trees or buildings [36]. The path loss induced power attenuation of users is assumed obey the product-distance law, which can be expressed as [19], [53]

$$L_m = (d_1 d_{2,m})^{-\alpha}, \tag{1}$$

where α represents the path loss exponent.

We consider a mmWave network, where the small-scale fading matrix of the BS-IRS links is modelled by the Nakagami fading channel as follows:

$$\mathbf{G} = \begin{bmatrix} g_{1,1} & \cdots & g_{1,M} \\ \vdots & \vdots & \vdots \\ g_{L,1} & \cdots & g_{L,M} \end{bmatrix}, \tag{2}$$

where $\mathbf{G}$ is a $L \times M$ matrix, $g_{l,m}$ denotes the channel gain between the m-th antenna at the BS and the l-th IRS element. The PDF of the elements is given by

$$f_1(x) = \frac{{t_1}^{t_1} x^{t_1-1}}{\Gamma(t_1)} e^{-t_1 x}, \tag{3}$$

where t_1 denotes the fading parameter.

Again, the Nakagami fading channel is used for evaluating the LoS link between the IRS elements and user m, which is given by

$$\mathbf{H}_m = \begin{bmatrix} h_{m,1,1} & \cdots & h_{m,1,L} \\ \vdots & \vdots & \vdots \\ h_{m,K,1} & \cdots & h_{m,K,L} \end{bmatrix}, \tag{4}$$

where $\mathbf{H}_m$ contains $K \times L$ elements associated with the fading parameter t_2, while $h_{m,k,l}$ denotes the channel gain between the l-th IRS element and the k-th antenna at user m. Based on the low-complexity channel estimation algorithms of [54], the global CSI is perfectly known at both the IRSs and the users.

Hence, the signal received at user m is given by

$$y = \mathbf{H}_m \mathbf{\Phi} \mathbf{G} \mathbf{P} \sqrt{L_m} + A, \tag{5}$$

where the reflection-coefficient matrix is a diagonal matrix. Similar to common assumptions, the reflection-coefficient matrix is denoted by $\mathbf{\Phi} \triangleq \text{diag}\left[\beta_1\phi_1, \beta_2\phi_2, \cdots, \beta_L\phi_L\right]$, where $\beta_l \in (0, 1]$ represents the amplitude coefficient of IRS elements [55]. The phase shift of IRS element l is denoted by $\phi_l = \exp(j\theta_l), j = \sqrt{-1}$, $\theta_l \in [0, 2\pi)$, where both the phase shifts and amplitude coefficients are perfectly known at the users [56]. In this article, it is assumed that both the amplitude coefficients and phase shifts of the IRS elements are continuous, which can be perfectly controlled. $\sqrt{L_m}$ denotes the path loss induced amplitude attenuation of user m Furthermore, in (5) A denotes the additive white Gaussian noise (AWGN) with variance σ^2. In order to provide access for multiple users with or without IRSs, the active beamforming weights are started by an identity matrix, where $\mathbf{P} = \mathbf{I}_M$. By doing so, the proposed active beamforming weights and detection vectors can be used without any further update in the case that 1) the direct links between the BS and users exist, while no reflected links exist; 2) the reflected links exist, while the direct links between the BS and users do not exist.

B. Passive Beamforming Design

Without loss of generality, a detection vector $\mathbf{v}_m$ is applied by user m to the received signal as follows:

$$\begin{aligned} \tilde{y}_m &= \mathbf{v}_m^{\mathrm{H}} \mathbf{H}_m \mathbf{\Phi} \mathbf{G} \mathbf{P} \sqrt{L_m} + \mathbf{v}_m^{\mathrm{H}} A \\ &= \mathbf{v}_m^{\mathrm{H}} \mathbf{H}_m \mathbf{\Phi} \mathbf{G} \sqrt{L_m} \mathbf{p}_m \\ &+ \underbrace{\sum_{i \neq m} \mathbf{v}_m^{\mathrm{H}} \mathbf{H}_m \mathbf{\Phi} \mathbf{G} \sqrt{L_m} \mathbf{p}_i}_{\text{interference}} + \mathbf{v}_m^{\mathrm{H}} A, \end{aligned} \tag{6}$$

where $\mathbf{v}_m$ is a $K \times 1$ vector.

In order to simultaneously serve all M users by L surfaces, we first define a $K \times L$ complex-valued matrix as:

$$\begin{aligned} &\bar{\mathbf{G}}_m \\ &= \begin{bmatrix} h_{m,1,1} g_{1,m} \beta_1 \phi_1 & \cdots & h_{m,1,L} g_{L,m} \beta_L \phi_L \\ \vdots & \vdots & \vdots \\ h_{m,K,1} g_{1,m} \beta_1 \phi_1 & \cdots & h_{m,K,L} g_{L,m} \beta_L \phi_L \end{bmatrix}. \end{aligned} \tag{7}$$

Since the superimposed signals aiming at user m cause strong interference, we aim for designing the passive beamforming weights with the goal of mitigating the interference at user m. Then, this problem can be formulated by stacking the channel gains of $\bar{\mathbf{G}}_1$ to $\bar{\mathbf{G}}_M$ as follows:

$$\bar{\mathbf{G}} = \begin{bmatrix} h_{1,1,1} g_{1,1} & \cdots & h_{1,1,L} g_{L,1} \\ \vdots & \vdots & \vdots \\ h_{1,K,1} g_{1,1} & \cdots & h_{1,K,L} g_{L,1} \\ h_{2,K,1} g_{1,2} & \cdots & h_{2,1,1} g_{L,2} \\ \vdots & & \vdots \\ h_{M,K,1} g_{1,M} & \cdots & h_{M,K,L} g_{L,M} \end{bmatrix}, \tag{8}$$

where $\bar{\mathbf{G}}$ contains $MK \times L$ elements.

In order to obtain the passive beamforming weights at the IRS, an object vector is defined as follows:

$$\mathbf{S} = \begin{bmatrix} s_{1,1} \\ s_{1,2} \\ \cdots \\ s_{M,K} \end{bmatrix}, \tag{9}$$

where $\mathbf{S}$ contains $MK \times 1$ elements, each of which can be obtained by $\begin{bmatrix} s_{m,1} \\ \vdots \\ s_{m,K} \end{bmatrix} = \bar{\mathbf{G}}_m \mathbf{1}_L$, which is a $L \times 1$ all

one vector. Hence, for example, the channel gain of the 1-st antenna at user m is given by:

$$\begin{aligned} s_{m,1} &= \left| \sum_{l=1}^{L} h_{m,1,l} g_{l,m} \beta_l \phi_l \right| \\ &\leq \left| \sum_{l=1}^{L} h_{m,1,l} g_{l,m} \beta_l \right|. \end{aligned} \tag{10}$$

We assume $\beta_l = 1$ for simplicity, and thereby the maximal achievable channel gain can be derived in the case that the reflected signals are co-phased as

$$s_{m,1} \leq \sum_{l=1}^{L} \left| h_{m,1,l} \right| \left| g_{l,m} \right|. \tag{11}$$

Hence, we can have the objective function of IRS elements as follows:

$$\begin{aligned} &\Phi_{\mathbf{v}} = \bar{\mathbf{G}}^{-1}\mathbf{S} \\ &subject\ to\ \theta_1 \cdots \theta_L \in [0, 2\pi) \\ &\beta_1 \cdots \beta_L \in (0, 1], \end{aligned} \tag{12}$$

where $\bar{\mathbf{G}}^{-1}$ represents the pseudo-inverse of the matrix, Φ_{v} can be decomposed into $\left[\begin{array}{ccc} \bar{\beta}_1\phi_1, & \cdots, & \bar{\beta}_L\phi_L \end{array} \right]^{\mathrm{T}}$, and $\bar{\beta}_l$ represents the unnormalized amplitude coefficients. Since the elements in $\bar{\mathbf{G}}$ are independent and unrelated, $\bar{\mathbf{G}}$ can be considered as a nonsingular matrix, which indicates that the pseudo-inverse of $\bar{\mathbf{G}}^{-1}$ does exist. Based on the above constraint we have $\beta_1, \cdots, \beta_L \in (0, 1]$, whereas the unnormalized amplitude coefficients derived in (12) may be higher than one, hence we normalize the amplitude coefficients as follows

$$\mathbf{\Phi} = \frac{\mathbf{\Phi_v}}{\beta_{\max}}, \tag{13}$$

where $\beta_{\max}$ can be derived by searching for the maximum amplitude coefficient of Φ_{v}[2].

Due to the fact that $rank(\bar{\mathbf{G}}) \leq MK$, no solutions exist for the case of $L < MK$ for passive beamforming. By contrast, when $L > MK$, an infinite number of homogeneous solutions exist for passive beamforming at the IRS elements, where the constraints of $\theta_l \in [0, 2\pi)$ and $\beta_l \in (0, 1]$, $\forall l = 1, \cdots, L$ can be satisfied.

By applying the proposed passive beamforming in (12), the effective channel gains can be derived by $\mathbf{v}_m^{\mathrm{H}}\mathbf{H}_m\mathbf{\Phi}\mathbf{G}$. Hence, the channel gain of the m-th user can be rewritten as

$$\mathbf{g}_m = \begin{bmatrix} \frac{1}{\beta_{\max}} \sum_{l=1}^{L} \left| h_{m,1,l} \right| \left| g_{l,m} \right| \\ \vdots \\ \frac{1}{\beta_{\max}} \sum_{l=1}^{L} \left| h_{m,K,l} \right| \left| g_{l,m} \right| \end{bmatrix}. \tag{14}$$

C. Detection Vector Design

The detection vectors of the users are designed by ensuring that they can i) mitigate the intra-cell interference; and ii) perform well both in IRS and non-IRS scenarios. We first focus our attention on the IRS scenario, since the BS-user links are blocked, the channel matrix of the m-th user can be transformed into a $K \times M$ matrix, which is given by

$$\hat{\mathbf{G}}_m = \mathbf{H}_m\mathbf{\Phi}\mathbf{G}. \tag{15}$$

hence the following constraint has to be met:

$$\mathbf{v}_m^{\mathrm{H}}\hat{\mathbf{G}}_m\mathbf{p}_i = \mathbf{0}, \tag{16}$$

for any $i \neq m$.

Since the active beamforming weights are elements of an identity matrix, the above constraint in (16) can be transformed into

$$\mathbf{v}_m^{\mathrm{H}}\hat{\mathbf{g}}_i = 0, \tag{17}$$

where $\hat{\mathbf{g}}_i$ is the i-th column of the effective channel matrix $\hat{\mathbf{G}}_m$ in (15). Hence, based on the zero-forcing design, the m-th column of $\hat{\mathbf{G}}_m$ can be removed. Hence we have

$$\tilde{\mathbf{G}}_m = \left[\begin{array}{ccccccc} \hat{\mathbf{g}}_1 & \cdots & \hat{\mathbf{g}}_{m-1} & \hat{\mathbf{g}}_{m+1} & \cdots & \hat{\mathbf{g}}_M \end{array} \right], \tag{18}$$

where $\tilde{\mathbf{G}}_m$ contains $K \times (M-1)$ elements. Thus, the constraint in (17) can be rewritten as follows:

$$\mathbf{v}_m^{\mathbf{H}}\tilde{\mathbf{G}}_m = \mathbf{0}. \tag{19}$$

Hence, we can obtain the detection vector of the m-th user from the null space of $\tilde{\mathbf{G}}_m$, which can be written as

$$\mathbf{v}_m = \mathbf{T}_m\mathbf{x}_m, \tag{20}$$

where $\mathbf{T}_m$ is derived by the left singular vectors of $\tilde{\mathbf{G}}_m$. We then use the classic maximal ratio combining (MRC) technique, hence $\mathbf{x}_m$ is given by

$$\mathbf{x}_m = \frac{\mathbf{T}_m^{\mathrm{H}}\mathbf{h}_m}{|\mathbf{T}_m^{\mathrm{H}}\mathbf{h}_m|}. \tag{21}$$

To ensure the existence of the left singular vector in (18), the number of TAs has to be lesser than the number of RAs, i.e. $K \geq M$. Otherwise, the solution does not exist. Note that more powerful, but more complex active beamformers can be designed for reducing the number of RAs, however, this is beyond the scope of this treatise.

Based on the active beamforming and DL user-detection vectors designed, the SNR of user m after detection can be written as:

$$SNR_m = \frac{\left| \mathbf{v}_m^{\mathrm{H}}\mathbf{g}_m \right|^2 (d_1 d_{2,m})^{-\alpha} p_b}{\left| \mathbf{v}_m^{\mathrm{H}} \right|^2 \sigma^2}, \tag{22}$$

where p_b represents the transmit power for user m, σ^2 denotes the AWGN power.

Since the detection vectors are normalized by that for user m, some further relevant observations are given by:

$$\left| \mathbf{v}_m^{\mathrm{H}} \right|^2 = \left(\frac{\left| \mathbf{T}_m\mathbf{T}_m^{\mathrm{H}} \right|}{\left| \mathbf{T}_m^{\mathrm{H}} \right|} \right)^2 = \left| \mathbf{T}_m^{\mathrm{H}} \right|^2, \tag{23}$$

and

$$\left| \mathbf{v}_m^{\mathrm{H}}\mathbf{g}_m \right|^2 = \left(\frac{\left| \mathbf{T}_m\mathbf{T}_m^{\mathrm{H}}\mathbf{g}_m^2 \right|}{\left| \mathbf{T}_m^{\mathrm{H}}\mathbf{g}_m \right|} \right)^2 = \left| \mathbf{T}_m^{\mathrm{H}}\mathbf{g}_m \right|^2. \tag{24}$$

Based on the effective channel gain given by (14) and noting

[2]Note that, since $\beta_{max} \geq 1$, the results derived may not represent the optimized solution.

that $\mathbf{T}_m^{\mathrm{H}}\mathbf{T}_m = \mathbf{I}_Q$ in (23) with $Q = K - M + 1$, the m-th user's channel gain is obtained by [52]

$$|\mathbf{g}_m| = \frac{1}{\beta_{\max}} \begin{bmatrix} \sum_{l=1}^{L} |h_{m,1,l}|\,|g_{l,m}| \\ \vdots \\ \sum_{l=1}^{L} |h_{m,Q,l}|\,|g_{l,m}| \end{bmatrix}. \tag{25}$$

Thus, the SNR of user m can be expressed as

$$SNR_m = \frac{\|\mathbf{g}_m\|^2 (d_1 d_{2,m})^{-\alpha} p_b}{\beta_{\max}^2 \|\mathrm{I}_Q\|_2^2 \sigma^2}. \tag{26}$$

In the non-IRS scenario, the BS-user links exist, and the small-scale fading matrix of the BS-user links is modelled by the Rayleigh fading channel as follows:

$$\mathbf{G}_m = \begin{bmatrix} g_{1,1} & \cdots & g_{1,M} \\ \vdots & \vdots & \vdots \\ g_{K,1} & \cdots & g_{K,M} \end{bmatrix}, \tag{27}$$

where $\mathbf{G}_m$ is a $K \times M$ matrix. Then, by utilizing similar steps to these spanning from (16) to (26), the active beamforming weights and detection vectors can be obtained in the non-IRS scenario.

III. Performance Analysis

In this section, we discuss the performance of the proposed MIMO-IRS network. The channel statistics derived for the high-SNR regime, the outage probabilities, ergodic rates, SE and EE are evaluated.

A. Channel Statistics

We first derive the effective channel statistics for the high-SNR regime of the proposed MIMO-IRS network. Let us assume that the users are distributed according to a BPP, where the IRS elements are co-located at the center of the disc. Then, the PDF of the user distances is written as

$$f_d(r) = \frac{2r}{(R^2 - r_0^2)}, \text{if} \quad r_0 < r < R. \tag{28}$$

Lemma 1. *Assume that the elements in $\mathbf{G}$ and $\mathbf{H}_m$ are i.i.d. with $t_1 \neq t_2$[3], respectively, and that M users are simultaneously served by L IRS elements with $L \geq K \geq M$. The PDF of the effective channel gain at user m in the high-SNR regime is given by*

$$f_{|\mathbf{g}_m|^2}(x) = \frac{\tilde{m}^L}{\Gamma(2t_s L)} x^{2t_s L - 1} e^{-2\sqrt{t_s t_l}x}, \tag{29}$$

where $t_s = \min\{t_1, t_2\}$, $t_l = \max\{t_1, t_2\}$, and $\tilde{m} = \frac{\sqrt{\pi} 4^{t_s - t_l + 1} (t_s t_l)^{t_s} \Gamma(2t_s)\Gamma(2t_l - 2t_s)}{\Gamma(t_s)\Gamma(t_l)\Gamma(t_s + t_l + 0.5)}$. Then, in the high-SNR regime, the cumulative density function (CDF) of the effective channel gain can be expressed as:

$$F_{|\mathbf{g}_m|^2}(x) = \frac{\tilde{m}^L (4 t_s t_l)^{-t_s L}}{\Gamma(2t_s L)} \times \gamma\left(2t_s L, 2\sqrt{t_s t_l} x\right). \tag{30}$$

Proof. Please refer to Appendix A. □

B. Outage Probability

The OP of the m-th user is given by

$$P_m = \mathbb{P}\left(\log_2(1 + SNR_m) < R_m\right), \tag{31}$$

where R_m denotes the target rate of user m.

Theorem 1. Assuming that the L IRS elements are located at the center of the disc for serving M users, the closed-form OP expression of user m is obtained by

$$\begin{aligned} P_{m,l} = {} & \tau_1 R^{\alpha a + 2} {}_2F_2\left(a, a + \delta_1; a + 1, a + \delta_1 + 1; -b_l R^{\alpha}\right) \\ & - \tau_1 r_0^{\alpha a + 2} {}_2F_2\left(a, a + \delta_1; a + 1, a + \delta_1 + 1; -b_l r_0^{\alpha}\right), \end{aligned} \tag{32}$$

where we have $\delta_{m,l} = \frac{\varepsilon_m \beta_{\max}^2 Q \sigma^2}{p_b}$, $\varepsilon_m = 2^{R_m} - 1$, $a = 2t_s L$, $b_l = 2\sqrt{t_s t_l}\delta_{m,l} d_1^{\alpha}$, $\delta_1 = \frac{1}{\alpha}$, $\varphi = \frac{2\tilde{m}^L (4 t_s t_l)^{-t_s L}}{\Gamma(2t_s L)\left(R^2 - r_0^2\right)}$, and $\tau_1 = \frac{\varphi b_l^a}{a(\alpha a + 2)}$.

Proof. Please refer to Appendix B. □

Since δ_m is a function of the maximum amplitude coefficients, it is hard to obtain analytical insights from (32). Thus, we turn our attention to finding the optimized solutions. In order to provide some fundamental engineering insights, we mainly focus our attention on the optimized scenario in the rest of this article, where $\beta_l = 1, \forall l$. It is worth noting that for the case of $K = M = 1$, the amplitude coefficients β_l and $\beta_{\max}$ can all be considered to be one and the maximum signal power can be obtained by appropriately adjusting the phase shifts. Thus, we formulate the upper bound of the approximated OP in the following Theorem.

Theorem 2. Assuming that the number of IRS elements is high enough, the upper bound of the approximated OP is given by

$$\begin{aligned} P_m = {} & \tau_1 R^{\alpha a + 2} {}_2F_2\left(a, a + \delta_1; a + 1, a + \delta_1 + 1; -b R^{\alpha}\right) \\ & - \tau_1 r_0^{\alpha a + 2} {}_2F_2\left(a, a + \delta_1; a + 1, a + \delta_1 + 1; -b r_0^{\alpha}\right), \end{aligned} \tag{33}$$

where we have $\delta_m = \frac{\varepsilon_m Q \sigma^2}{p_b}$, $b = 2\sqrt{t_s t_l}\delta_m d_1^{\alpha}$, and $\tau_1 = \frac{\varphi b^a}{a(\alpha a + 2)}$.

Proof. Similar to Appendix B, the results in (33) can be readily proved. □

It is however quite challenging to directly obtain engineering insights from (33) due to the Gauss hypergeometric function, hence the asymptotic behavior is analyzed in the high-SNR regime in the case of $\frac{p_b}{\sigma^2} \to \infty$.

[3]Since both the BS and the IRSs are part of the infrastructure, whereas the users are randomly located on the ground, the fading environments of the BS-IRS links are usually stronger than that of the IRS-user links.

Corollary 1. Assuming that $bR_{\max}^{\alpha} < 1$, the upper bound of closed-form asymptotic OP expression of user m is given by

$$\bar{P}_m = \frac{\varphi b^{n+a}}{a(\alpha a+2)} \sum_{n=0}^{\infty} t_{n1} \left(R^{\alpha a+\alpha n+2} - r_0^{\alpha a+\alpha n+2} \right), \quad (34)$$

where $t_{n1} = \frac{(a)_n (a+\delta_1)_n}{(a+1)_n (a+\delta_1+1)_n n!}$, $(x)_n$ represents the Pochhammer symbol [50], which can be calculated as $\frac{\Gamma(x+n)}{\Gamma(x)}$.

Proof. Please refer to Appendix C. □

Proposition 1. From **Corollary 1**, we can determine the diversity order by utilizing the asymptotic results, and the diversity order of user m in the proposed MIMO-IRS network is given by

$$d_m = -\lim_{\frac{P_b}{\sigma^2} \to \infty} \frac{\log \bar{P}_m}{\log \frac{P_b}{\sigma^2}} \approx a = 2t_s L. \quad (35)$$

Proof. Based on the results derived in (34), and on the definition of diversity order, we have

$$d_m \approx -\lim_{\frac{P_b}{\sigma^2} \to \infty} \frac{\log \sum_{n=0}^{\infty} \left(\frac{\sigma^2}{P_b} \right)^{n+a}}{\log \frac{P_b}{\sigma^2}}. \quad (36)$$

Due to the fact that $\frac{P_b}{\sigma^2} \to \infty$ and $\delta_m \to 0$, and because the maximal component can be obtained in the case of $n = 0$ in (36), we have

$$d_m = n + a = a. \quad (37)$$

The proof is complete. □

Remark 1. *The results in* (35) *demonstrate that both the fading links between the IRS elements and the users as well as that between the BS and IRS elements significantly affect the OP. Note that when $Q \to \infty$, the diversity order of the proposed network approaches $2t_s L$.*

Remark 2. *For the case of $M = 1$, the minimal diversity order of the proposed network is $2t_s L$, which indicates that having more IRS elements reduces the OP. Note that the minimum diversity order is 2 in the case of $t_1 = L = M = K = 1$ and $t_2 > 1$, i.e. $\min(d_m) = 2$.*

Since we have LoS links between the BS and IRSs, and the 0-th ordered element is the main component of the asymptotic result in (34). The following fundamental numerical insight may be inferred:

Corollary 2. Assuming that $M = K = t_2 = 1$, $t_1 \to \infty$, and $r_0 = 0$, the 0-th ordered element in terms of the asymptotic OP of user m is given by

$$\bar{P}_{m,0} = \frac{2\varepsilon_m^L (d_1 R)^{L\alpha}}{(L\alpha+2)L!}. \quad (38)$$

Remark 3. *The results in* (38) *indicate that the diversity order is N in the case of the proposed MIMO-IRS network for $M = K = t_2 = 1$, $t_1 \to \infty$.*

Remark 4. *We also provide a basic engineering insight relying on the proposed network, where $M = K = 1$. It is reasonable to assume that no LoS link exists between the IRSs and the user, where the Nakagami fading parameter is $t_2 = 1$. Thus, based on the results in* (35)*, we can readily infer that the diversity order approaches $d_m = 2L$.*

C. Ergodic Rate

Since the ergodic rate is capable of characterising the network's SE and EE, we analyze the ergodic rate of the typical user m. In order to obtain a tractable ergodic rate expression, we first provide the approximated channel gain $\hat{\mathbf{g}}_m$ of our MIMO-IRS network.

Lemma 2. *Based on the insights of [57], the classic Gamma distribution is assumed. The approximated distribution of the channel gain at the m-th user is given by*

$$\left\| \hat{\mathbf{G}}_m \right\|^2 \sim \Gamma\left(\frac{LQ}{t_h}, t_h \right), \quad (39)$$

where $t_h = \frac{(1+t_1+Qt_2)}{t_1 t_2}$.

Proof. Please refer to Appendix D. □

We then analyze the exact ergodic rate expressions by relying on the Meijer-G functions in the following Theorem.

Theorem 3. The ergodic rate of the m-th user can be expressed in closed-form:

$$\begin{aligned} \bar{R}_m = & \frac{\varphi c^{-\delta_2}}{2\ln(2)} \mathrm{G}_{\,2,3}^{\,3,1} \left(\begin{matrix} \delta_2, 1 \\ \delta_2, 0, a+\delta_2 \end{matrix} \middle| cr_0^{\alpha} \right) \\ & + \frac{\varphi R^2}{2\ln(2)} \mathrm{G}_{\,2,3}^{\,3,1} \left(\begin{matrix} 0, 1 \\ 0, 0, a \end{matrix} \middle| cR^{\alpha} \right) \\ & - \frac{\varphi r_0^2}{2\ln(2)} \mathrm{G}_{\,2,3}^{\,3,1} \left(\begin{matrix} 0, 1 \\ 0, 0, a \end{matrix} \middle| cr_0^{\alpha} \right) \\ & - \frac{\varphi c^{-\delta_2}}{2\ln(2)} \mathrm{G}_{\,2,3}^{\,3,1} \left(\begin{matrix} \delta_2, 1 \\ \delta_2, 0, a+\delta_2 \end{matrix} \middle| cR^{\alpha} \right), \end{aligned} \quad (40)$$

where $c = \frac{Q\sigma^2}{t_h p_b}$.

Proof. Please refer to Appendix D. □

To illustrate the increasing slope of the ergodic rate, the high-SNR slope is worth estimating, which can be expressed as

$$Z = -\lim_{\frac{p_b}{\sigma^2} \to \infty} \frac{\bar{R}_m}{\log_2\left(1 + \frac{p_b}{\sigma^2}\right)}. \quad (41)$$

Proposition 2. By substituting (40) into (41), the high-SNR slope of the m-th user is derived as

$$Z = 1. \quad (42)$$

Proof. Note that we have $Z = \frac{d\bar{R}_m}{d\log_2\left(\frac{p_b}{\rho^2}\right)} = \ln(2) \frac{p_b}{\rho^2} \frac{d\bar{R}_m}{d\left(\frac{p_b}{\rho^2}\right)} = 1$, and this completes the proof. □

Remark 5. (42) *indicates that the number of IRS elements has no impact on the high-SNR slope, which is one.*

Remark 6. (42) *indicates that the high-SNR slope is one, which is not affected by the number of TAs/RAs neither is not influenced by the fading environments.*

D. SE and EE

Finally, the SE and EE are obtained in the following two Propositions.

Proposition 3. Based on the derived ergodic rates in (40), an tractable SE expression can be derived as

$$SE = \sum_{m=1}^{M} \bar{R}_m. \tag{43}$$

Since EE is a critical performance indicator, the power consumption can be modelled as [58]

$$P_e = P_{\mathrm{B,s}} + MP_{\mathrm{U}} + Mp_b\varepsilon_b + LP_L, \tag{44}$$

where the power consumption and the efficiency of the power amplifier at the BS are denoted by $P_{\mathrm{B,s}}$ and ε_b, respectively. The power consumption of each user and each IRS element are denoted by P_{U} and P_L, respectively.

Proposition 4. The EE of the proposed MIMO-IRS network can be formulated as:

$$\Theta_{EE} = \frac{SE}{P_e}, \tag{45}$$

where S and P_e are obtained from (43) *and* (45)*, respectively.*

IV. Numerical Results

Numerical results for the performance evaluation of our proposed MIMO-IRS network are presented in this section. Monte Carlo simulations are conducted to confirm the correctness of the analytical results. The transmit bandwidth D is set to 100 MHz, and the power of the AWGN is set to $-174+10\log_{10}D$ dBm. The path loss index α is set to 3, and the power attenuation at the reference distance is set to -30 dB. The minimum distance and the reference distance are both set to one meter. The length of the BS-IRS link is set to $d_1 = 30$m the disc radius R is set to 100m, and the target rate R_m is set to 1.5 bits per channel use (BPCU). In this article, the number of users and the number of TAs are both set to M. The Nakagami fading parameters of $t_1 = t_2 = 1$ and $t_1 > 1, t_2 > 1$ represent Non-LoS (NLoS) and LoS links, respectively. Since the fading parameters and the number of IRS elements are related to the diversity orders, the fading parameters are set to $t_1 = 1, 2, 3$ and $t_2 = 1, 2, 3$ for simplicity. To mitigate the computational complexity, the number of Monte Carlo iterations is limited to 10^6. The main simulation parameters are summarized in Table IV.

We first evaluate the OP impacted by the number of IRS elements in Fig. 2. In order to illustrate the performance gain due to increasing the number of IRS elements, the numbers of TAs and RAs are set to 1 for simplicity. The solid and dashed curves represent the analytical results and asymptotic results, respectively. There is a large gap between the simulation and analytical results because that the results are derived as high-SNR approximations. However, in the high-SNR regime, we have close agreement between the simulation and analytical results is closely. Observe that the OP increases with the number of IRS elements because the channel gain is improved by the increased diversity order. For example, as shown by the blue curve and green curve, as well as by the results in (35), the diversity orders are 4 and 6 for the cases of $L = 2$ and $L = 3$, respectively. We can observe that the slope of the curves increases with the number of IRS elements, which verifies our **Remark 2**.

TABLE IV:
TABLE OF SIMULATION PARAMETERS

Path loss exponent	$\alpha = 3$
The distance of the BS-IRS links	$d_1 = 30$
The radius of the disc	$R = 100$
The target rate of user m	$R_m = 1.5$
Fading parameter of the BS-IRS links	$t_1 = 1, 2, 3$
Fading parameter of the IRS-user links	$t_2 = 1, 2, 3$
The number of users	M
The number of antennas at the BS	M
Bandwidth	100MHz
The power of the AWGN	-94dBm

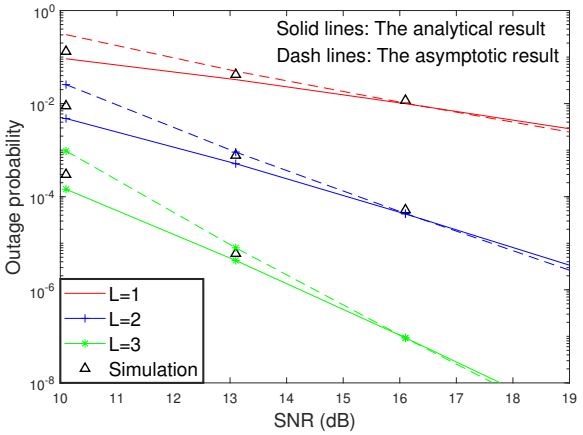

Fig. 2: OP of user m with $M = K = 1$, $t_1 = 2, t_2 = 1$. The analytical results and asymptotic results are calculated from (33) and (34), respectively.

In FIg. 3, we evaluate the OP of the m-th user for different fading parameters. We can see that as the SNR increases, the OP decreases. We can also observe that stronger LoS environments typically decrease the OP. Observe that the fading parameter of the IRS-user link has almost no effect on the OP, which mainly depends on that of the BS-IRS link. This phenomenon verifies the insights gleaned from **Remark 1**. Note that the slope of the curves is governed by t_1, which verifies that the diversity orders of the schemes mainly depend on t_1, when the effective channel gain is high enough. This also validates the insights gleaned from **Remark 2**.

We evaluate the ergodic rate of the m-th user in Fig. 4. The solid and dashed curves represent the analytical and simulation results, respectively. By comparing the black curve and cyan curve, one can observe that the ergodic rate of users is only moderately impacted by the LoS components of the IRS-users links, whereas the LoS components of the BS-IRSs improve the ergodic rate. In addition, the high-SNR slope of the m-th user is one, which illustrates that the number of IRS elements has no impact on the high-SNR slope of users.

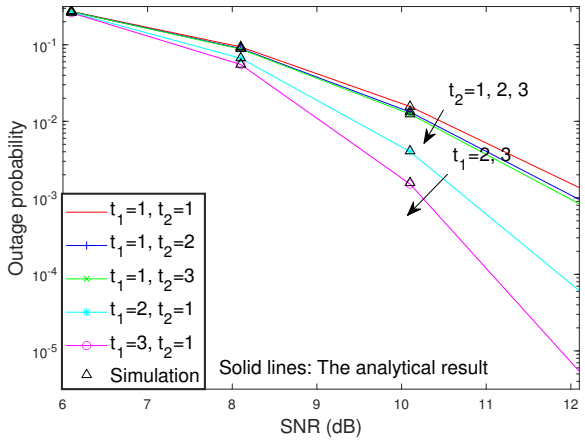

Fig. 3: OP of the m-th user with $t_1, t_2 = 1, 2, 3$. The number of TAs and RAs, as well as IRS elements are set to $M = 1, K = 10$, $L = 10$, respectively. The analytical and asymptotic results both are calculated by (39).

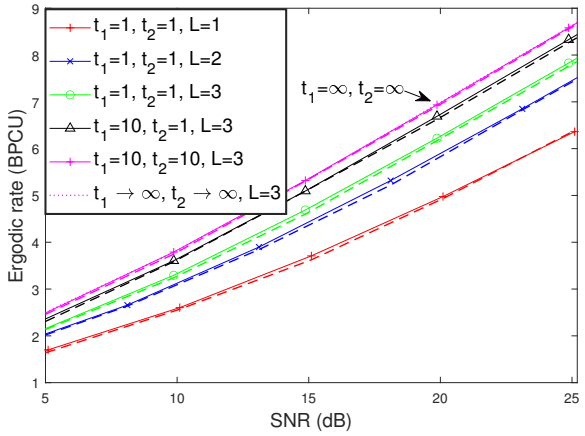

Fig. 4: Ergodic rate of the m-th user in the case of $M = 1$.

Furthermore, by employing more IRS elements, the ergodic rate can be significantly increased, which is due to the fact that the number of IRS elements is capable of beneficially improving the spatial diversity gain.

Based on the insights gleaned from [19], [59], the achievable rate of two alternative half-duplex relay setups, namely of the classic amplify-then-forward (AF) relay and of decode-then-forward (DF) relay setup are evaluated, where the transmission is divided into two equal-duration phases[4]. It is assumed that the BS, relay and user are equipped with a single antenna in both the AF-relay and DF-relay setups. The length of the BS-IRS link is set to 100 meters. We first evaluate the achievable rate of the AF-relay setup, where the AF-relay simply amplifies the received signal without decoding. Therefore, on the one hand, the SE of the AF-relay setup can be written as

$$R_{\mathrm{AF}} = \mathbb{E}\left\{\frac{1}{2}\log_2\left(1 + SINR_{\mathrm{AF}}\right)\right\}, \tag{46}$$

[4]Since there is no BS-user link, full-duplex relaying is not considered in this treatise, because of the selected simulation parameters of the length, path loss exponents and self-interference coefficient.

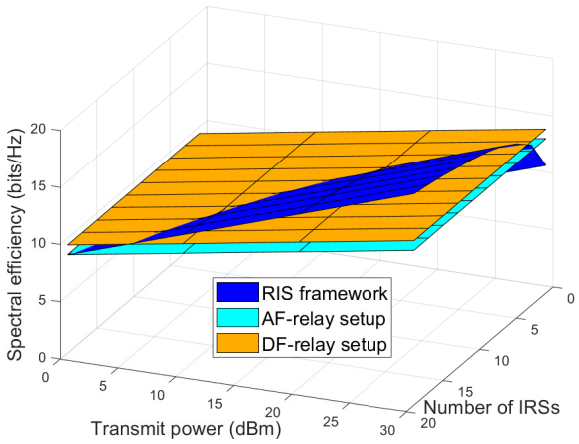

Fig. 5: Spectral efficiency of the MIMO-IRS network, AF-relay and DF-relay setup versus the number of IRS elements and the total transmit power with $t_1 = 3, t_2 = 1$, where the number of TAs/RAs are set to $M = 1, K = 1$.

where p_d denotes the transmit power of the relay, $SINR_{\mathrm{AF}} = \frac{\varepsilon_a (d_1 d_{2,m})^{-\alpha} |h_1|^2 |h_2|^2}{\sigma^2 (1 + \varepsilon_a d_{2,m}^{-\alpha} |h_2|^2)}$, and ε_a denotes the amplification coefficient of the AF-relay with $\varepsilon_a = \frac{p_d}{p_b} d_1^{\alpha} |h_1|^{-2}$. Note that the AWGN of the BS to IRS link is also amplified by the AF-relay.

On the other hand, the achievable rate expression of the DF-relay setup is more complicated. The DF-relay has to decode the signal received from the BS, and the achievable rate can be written as follows:

$$R_{\mathrm{DF},1} = \mathbb{E}\left\{\frac{1}{2}\log_2\left(1 + SNR_{\mathrm{DF1}}\right)\right\}, \tag{47}$$

where $SNR_{\mathrm{DF1}} = \frac{p_b d_1^{-\alpha} |h_1|^2}{\sigma^2}$. Then, the user decodes the signal retransmitted by the DF-relay at a rate of:

$$R_{\mathrm{DF},2} = \mathbb{E}\left\{\frac{1}{2}\log_2\left(1 + SNR_{\mathrm{DF2}}\right)\right\}, \tag{48}$$

where $SNR_{\mathrm{DF2}} = \frac{p_d d_2^{-\alpha} |h_2|^2}{\sigma^2}$. Thus, the achievable rate of the DF-relay setup can be rewritten as

$$R_{\mathrm{DF}} = \min\{R_{\mathrm{DF},1}, R_{\mathrm{DF},2}\}. \tag{49}$$

Here, we evaluate the SE of both our IRS network, as well as that of the AF-relay and DF-relay setups in Fig. 5. The results of the AF-relay and DF-relay setup are derived from (46) and (49), respectively. In order to compare our IRS network, as well as the AF-relay and DF-relay setups under fair conditions, the total transmit powers p_{tot} are set to be identical. Explicitly, the transmit power of the IRS network is set to $p_b = p_{tot}$ dBm, while the transmit powers of both the AF-relay and DF-relay are set to $(p_d + p_b) = p_{tot}$ dBm. The optimal power split strategies of both the AF and DF relays are based on [19] for achieving the optimal SE. We can see that the rate difference between the MIMO-IRS network, AF-relay and DF-relay setup becomes smaller, when the number of IRS elements is increased. Observe that for the case of $L = 15$, the proposed MIMO-IRS network is capable of outperforming the AF-relay and DF-relay setups, which indicates that the MIMO-IRS network becomes more competitive, when the number of

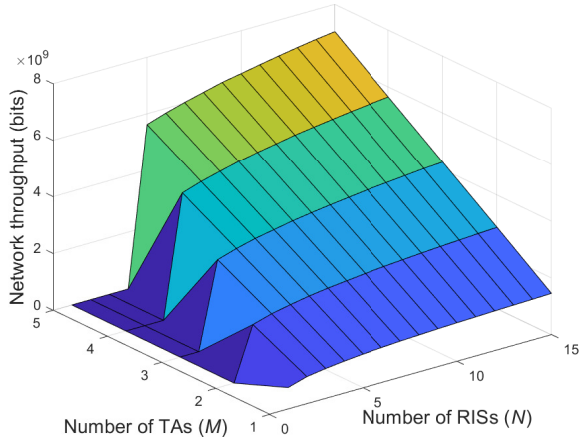

Fig. 6: Network throughput versus the number of IRS elements and TAs, as well as RAs with $K = M$. The LoS links are associated with $t_1 = t_2 = 2$.

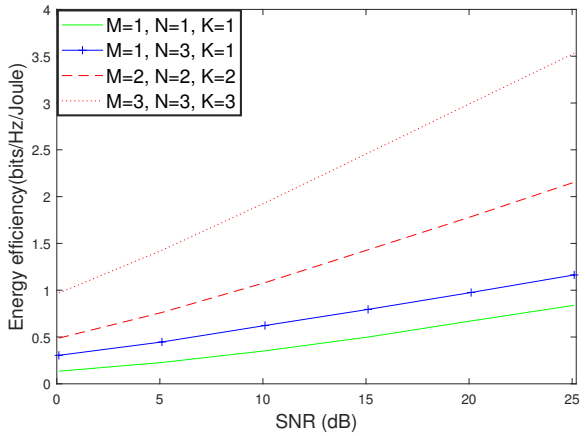

Fig. 7: The network's EE with $t_1 = 5, t_2 = 1$. The amplifier efficiency ε_b at the BS is set to 1.2. The static power at the BS $P_{\mathrm{B,s}}$ and users P_{U} are set to 9 dBW and 10 dBm, respectively. $P_L = 10$ dBm represents the power consumption of each IRS element.

IRS elements is high enough. One can also observe that the proposed MIMO-IRS network is more sensitive to the total transmit power, which is due to the fact that at the current state-of-the-art, the IRS elements cannot amplify the received signals.

The network throughput is illustrated in Fig. 6 in the case of $p_b = 30$ dBm. The results illustrate that the network throughput increases with the number of TAs, which is caused by the fact that the BS simultaneously serves more users, thereby improving the SE. Furthermore, the networks throughput monotonically increases as the number of TAs and of IRS elements increases. Note that no solution exists at the IRSs in the case of $L < MK$, hence the network's SE is zero.

The network's EE is evaluated in Fig. 7. Observe that as the number of TAs, RAs, and IRS elements increases, the network's EE increases, which is because increasing the number of RAs, TAs and IRS elements is capable of increasing the spatial diversity gain. Moreover, the slope of the network's EE is improved by improving the number of RAs, TAs and IRS elements.

V. Conclusions

In this paper, IRS-aided MIMO networks were derived. We then designed both the detection vectors and passive beamforming at the users and the IRSs, respectively, where the proposed network performs well both in IRS and non-IRS scenarios. Furthermore, we derived the closed-form channel characteristics, outage probabilities, ergodic rates, SEs and EEs. In NG networks, multiple IRS arrays could be deployed as part of the infrastructure. Therefore, a promising future research direction is distributed IRS networks, where multiple IRS arrays are beneficially distributed on the facades of different buildings located in different areas. Based on the insights from [11], [47], another important future direction of IRS and stochastic geometry research is to model the location of users in a restricted geographic area.

Appendix A: Proof of Lemma 1

Since the elements of $|\mathbf{H}_m|$ and $|\mathbf{G}|$ are i.i.d., according to [23], the PDF of the product of two Nakagami-m random variables can be calculated as

$$f_{|g_m|^2}(x) = \frac{4(t_s t_l)^{\frac{t_s+t_l}{2}}}{\Gamma(t_s)\Gamma(t_l)} x^{t_s+t_l-1} \times I_{t_s-t_l}\left(2\sqrt{t_s t_l}x\right), \tag{A.1}$$

where $I_\alpha(\cdot)$ denotes the modified Bessel function of the second kind. Since (A.1) contains the modified Bessel function of the second kind, which is hard to calculate, hence we use the Laplace transform of the PDF, which can be derived as

$$L_{|\mathbf{g}_m|^2}(s) = \mathbb{E}\left(e^{-s\|\hat{\mathrm{g}}_m\|_2^2}\right) = \frac{4(t_s t_l)^{\frac{t_s+t_l}{2}}}{\Gamma(t_s)\Gamma(t_l)} \times \int_0^\infty x^{t_s+t_l-1} e^{-sx} I_{t_s-t_l}\left(2\sqrt{t_s t_l}x\right) dx. \tag{A.2}$$

By utilizing [50, eq. (6.621.3)], (A.2) can be further transformed into

$$L_{|\mathbf{g}_m|^2}(s) = \bar{m}\left(s + 2\sqrt{t_s t_l}\right)^{-2t_s} \times F\left(2t_s, t_s - t_l + 0.5; t_s + t_l + 0.5; \frac{s - 2\sqrt{t_s t_l}}{s + 2\sqrt{t_s t_l}}\right), \tag{A.3}$$

where $\bar{m} = \frac{\sqrt{\pi}4^{t_s-t_l+1}(t_s t_l)^{t_s}\Gamma(2t_s)\Gamma(2t_l)}{\Gamma(t_s)\Gamma(t_l)\Gamma(t_s+t_l+0.5)}$, and $F(\cdot,\cdot;\cdot;\cdot)$ represents the hypergeometric series.

We then focus on the high-SNR regime, where we have $\frac{P_b}{\sigma^2} \to \infty$ and $s \to \infty$. Then, upon assuming $t_1 \neq t_2$, the Laplace transform can be rewritten as

$$L_{|\mathbf{g}_m|^2}(s) = \tilde{m}\left(s + 2\sqrt{t_s t_l}\right)^{-2t_s}. \tag{A.4}$$

Since the reflected signals are i.i.d., the overall effective channel gain can be given by

$$L_{|\hat{\mathrm{g}}_m|^2}(s) = \tilde{m}^L\left(s + 2\sqrt{t_s t_l}\right)^{-2t_s L}. \tag{A.5}$$

Based on the inverse Laplace transform for (A.5), the PDF and CDF in the high-SNR regime can be obtained in (39), and hence we complete the proof.

APPENDIX B: PROOF OF THEOREM 1

We first handle the OP defined of user m in (31), which can be rewritten as

$$P_{m,l} = \mathbb{P}\left(\left|\mathrm{g}_m\right|^2 < \delta_{m,l}(d_1 d_{2,m})^{\alpha}\right). \tag{B.1}$$

Then, based on the channel statistics derived in (29) and on the distance distribution in (28), the OP can be transformed into

$$\begin{aligned} P_{m,l} = &\frac{2\tilde{m}^L (4t_s t_l)^{-t_s L}}{\Gamma(2t_s L)\left(R^2 - r_0^2\right)} \\ &\times \int_{r_0}^{R} \gamma\left(2t_s L, 2\sqrt{t_s t_l}\delta_{m,l} d_1^{\alpha} r^{\alpha}\right) r dr. \end{aligned} \tag{B.2}$$

By some further algebraic manipulations, we arrive at:

$$P_{m,l} \overset{(c)}{=} \varphi b^{-\delta_1} \int_{br_0^{\alpha}}^{bR^{\alpha}} \gamma(a, bx) x^{\delta_1} dx, \tag{B.3}$$

where (c) is obtained by substituting $x = br^{\alpha}$.

Then, based on [50], the OP can be calculated as

$$\begin{aligned} P_{m,l} = &\frac{\varphi b^a R^{\alpha a+2}}{a(\alpha a+2)} {}_2F_2\left(a, a+\delta_2; a+1, a+\delta_2+1; -bR^{\alpha}\right) \\ &- \frac{\varphi b^a r_0^{\alpha a+2}}{a(\alpha a+2)} {}_2F_2\left(a, a+\delta_2; a+1, a+\delta_2+1; -br_0^{\alpha}\right). \end{aligned} \tag{B.4}$$

Thus, the closed-form OP expression can be obtained as in (32), and the proof is complete.

APPENDIX C: PROOF OF COROLLARY 1

For the case of $bR^{\alpha} < 1$, the hypergeometric function can be expanded to

$$\begin{aligned} &{}_2F_2\left(a, a+\delta_1; a+1, a+\delta_1+1; -bR^{\alpha}\right) \\ &= \sum_{n=0}^{\infty} \left(\frac{(a)_n (a+\delta_1)_n}{(a+1)_n (a+\delta_1+1)_n n!}\right) b^n R^{\alpha n}. \end{aligned} \tag{C.1}$$

Thus, we can readily arrive at the asymptotic result of

$$\bar{P}_m = \frac{\varphi}{a(\alpha a+2)} \sum_{n=0}^{\infty} t_{n1} b^{n+a} \left(R^{\alpha a+\alpha n+2} - r_0^{\alpha a+\alpha n+2}\right). \tag{C.2}$$

We then can derive the desired result by algebraic manipulations in (34). The proof is complete.

APPENDIX D: PROOF OF LEMMA 2

Since the elements of $|\mathbf{H}_m|$ and $|\mathbf{G}|$ are i.i.d., we have the following inequations of the m-th user as

$$\begin{aligned} \left|\mathbf{g}_m\right|^2 &= \left(\sum_{k=1}^{K}\sum_{l=1}^{L} |h_{m,k,l} g_{l,m}|\right)^2 \\ &\geq \sum_{k=1}^{K}\sum_{l=1}^{L} |h_{m,k,l}|^2 |g_{l,m}|^2. \end{aligned} \tag{D.1}$$

Then, based on the property of Nakagami distribution, we can have:

$$\left(\sum_{k=1}^{K} |h_{m,k,l}|^2\right) \sim \mathcal{RV}\left(K, \frac{K}{t_2}\right). \tag{D.2}$$

Then the mean and variance in the case of $L = 1$ can be expressed as

$$\mathbb{E}\left(\sum_{k=1}^{K} |h_{m,k,l}|^2\right) \mathbb{E}\left(\left|\mathrm{g}_{1,m}\right|^2\right) = K, \tag{D.3}$$

and

$$V = \frac{K(1 + t_1 + Kt_2)}{t_1 t_2}. \tag{D.4}$$

Hence, by utilizing zero-forcing based detection vectors, the mean and variance is obtained as

$$\left\|\hat{\mathbf{G}}_m\right\|^2 \sim \mathcal{RV}\left(LQ, LQt_h\right), \tag{D.5}$$

where $t_h = \frac{(1+t_1+Qt_2)}{t_1 t_2}$. Hence, the proof is complete.

APPENDIX E: PROOF OF THEOREM 3

We initiate by providing the definition of ergodic rate as follows:

$$\begin{aligned} R_{m,e} &= \mathbb{E}\left\{\log_2\left(1 + SNR_m(x)\right)\right\} \\ &= -\int_0^{\infty} \log_2(1+x) d\left(1 - F(x)\right). \end{aligned} \tag{E.1}$$

By utilizing the results of CDF, we set

$$\lambda = 1 - F(x) = \varphi \int_{r_0}^{R} \Gamma_u\left(a, cxr^{\alpha}\right) r dr, \tag{E.2}$$

where the upper incomplete Gamma function is denoted by $\Gamma_u(,)$.

We then substitute $u = cxr^{\alpha}$ into (E.2), λ is rewritten as:

$$\lambda = \frac{\varphi (cx)^{-\delta_2}}{\alpha} \int_{cxr_0^{\alpha}}^{cxR^{\alpha}} \Gamma_u(a, u) u^{\delta_2 - 1} du. \tag{E.3}$$

By using upper incomplete Gamma function, λ is derived as

$$\begin{aligned} \lambda = &\frac{\varphi}{2} R^2 \Gamma_u\left(a, cR^{\alpha}x\right) - \frac{\varphi}{2}(cx)^{-\delta_2} \Gamma_u\left(a+\delta_2, cR^{\alpha}x\right) \\ &- \frac{\varphi}{2} r_0^2 \Gamma_u\left(a, cr_0^{\alpha}x\right) + \frac{\varphi}{2}(cx)^{-\delta_2} \Gamma_u\left(a+\delta_2, cr_0^{\alpha}x\right). \end{aligned} \tag{E.4}$$

To obtain tractable ergodic rates, the upper incomplete Gamma function are transformed into the Meijer-G function [50] as

$$\Gamma_u\left(a, cR^{\alpha}x\right) = \mathrm{G}_{1,2}^{2,0}\left(\begin{matrix} 1 \\ a, 0 \end{matrix} \middle| cR^{\alpha}x\right). \tag{E.5}$$

Then, the ergodic rate of the m-th user is obtained as [50]

$$\begin{aligned}\int_0^\infty \frac{\lambda}{1+x}dx = &\frac{\varphi}{2}R^2 \mathrm{G}_{\,2,3}^{\,3,1}\left(\begin{array}{c} 0,1 \\ 0,0,a \end{array}\middle| cR^\alpha\right) \\ &- \frac{\varphi}{2}c^{-\delta_2}\mathrm{G}_{\,2,3}^{\,3,1}\left(\begin{array}{c} \delta_2,1 \\ \delta_2,0,a+\delta_2 \end{array}\middle| cR^\alpha\right) \\ &- \frac{\varphi}{2}r_0^2\mathrm{G}_{\,2,3}^{\,3,1}\left(\begin{array}{c} 0,1 \\ 0,0,a \end{array}\middle| cr_0^\alpha\right) \\ &+ \frac{\varphi}{2}c^{-\delta_2}\mathrm{G}_{\,2,3}^{\,3,1}\left(\begin{array}{c} \delta_2,1 \\ \delta_2,0,a+\delta_2 \end{array}\middle| cr_0^\alpha\right).\end{aligned} \tag{E.6}$$

Thus, we can derive the ergodic rate in (40), which completes the proof.

REFERENCES

[1] S. Lien, S. Shieh, Y. Huang, B. Su, Y. Hsu, and H. Wei, "5G new radio: Waveform, frame structure, multiple access, and initial access," *IEEE Commun. Mag.*, vol. 55, no. 6, pp. 64–71, Jun. 2017.

[2] S. Parkvall, E. Dahlman, A. Furuskar, and M. Frenne, "NR: The new 5G radio access technology," *IEEE Commun. Standards Mag.*, vol. 1, no. 4, pp. 24–30, Dec. 2017.

[3] T. Bai and R. W. Heath, "Coverage and rate analysis for millimeter-wave cellular networks," *IEEE Trans. Wireless Commun.*, vol. 14, no. 2, pp. 1100–1114, Feb. 2015.

[4] E. Björnson, ö. özdogan, and E. G. Larsson, "Intelligent reflecting surface versus decode-and-forward: How large surfaces are needed to beat relaying?" *IEEE Wireless Commun. Lett.*, vol. 9, no. 2, pp. 244–248, Feb. 2020.

[5] Y. Liang, R. Long, Q. Zhang, J. Chen, H. V. Cheng, and H. Guo, "Large intelligent surface/antennas (LISA): Making reflective radios smart," *Journal of Communications and Information Networks*, vol. 4, no. 2, pp. 40–50, Jun. 2019.

[6] S. Hu, F. Rusek, and O. Edfors, "Beyond massive MIMO: The potential of data transmission with large intelligent surfaces," *IEEE Trans. Signal Processing*, vol. 66, no. 10, pp. 2746–2758, May 2018.

[7] ——, "Beyond massive MIMO: The potential of positioning with large intelligent surfaces," *IEEE Trans. Signal Processing*, vol. 66, no. 7, pp. 1761–1774, Apr. 2018.

[8] T. Hou, Y. Liu, Z. Song, X. Sun, and Y. Chen, "Multiple antenna aided NOMA in UAV networks: A stochastic geometry approach," *IEEE Trans. Commun.*, vol. 67, no. 2, pp. 1031–1044, Feb. 2019.

[9] X. Gao, P. Wang, D. Niyato, K. Yang, and J. An, "Auction-based time scheduling for backscatter-aided RF-powered cognitive radio networks," *IEEE Trans. Wireless Commun.*, vol. 18, no. 3, pp. 1684–1697, Mar. 2019.

[10] M. D. Renzo *et al.*, "Smart radio environments empowered by AI reconfigurable meta-surfaces: An idea whose time has come," *J. Wireless Comm. Network*, vol. 129, May 2019.

[11] M. D. Renzo and J. Song, "Reflection probability in wireless networks with metasurface-coated environmental objects: An approach based on random spatial processes," *J. Wireless Comm. Network*, vol. 99, Apr. 2019.

[12] J. Zhao, "A survey of intelligent reflecting surfaces (IRSs): Towards 6G wireless communication networks with massive MIMO 2.0," *arXiv*, vol. 1907.04789v2, pp. 1–1, Jul. 2019.

[13] T. Bai, C. Pan, Y. Deng, M. Elkashlan, A. Nallanathan, and L. Hanzo, "Latency minimization for intelligent reflecting surface aided mobile edge computing," *IEEE Journal on Selected Areas in Communications*, vol. 38, no. 11, pp. 2666–2682, Nov. 2020.

[14] C. Pan, H. Ren, K. Wang, W. Xu, M. Elkashlan, A. Nallanathan, and L. Hanzo, "Multicell MIMO communications relying on intelligent reflecting surfaces," *IEEE Trans. Wireless Commun.*, vol. 19, no. 8, pp. 5218–5233, Aug. 2020.

[15] C. Pan, H. Ren, K. Wang, M. Elkashlan, A. Nallanathan, J. Wang, and L. Hanzo, "Intelligent reflecting surface aided MIMO broadcasting for simultaneous wireless information and power transfer," *IEEE Journal on Selected Areas in Communications*, vol. 38, no. 8, pp. 1719–1734, Aug. 2020.

[16] X. Guan, Q. Wu, and R. Zhang, "Intelligent reflecting surface assisted secrecy communication: Is artificial noise helpful or not?" *IEEE Wireless Commun. Lett.*, vol. 9, no. 6, pp. 778–782, Jun. 2020.

[17] Q. Wu and R. Zhang, "Towards smart and reconfigurable environment: Intelligent reflecting surface aided wireless network," *IEEE Commun. Mag.*, vol. 58, no. 1, pp. 106–112, Jan. 2020.

[18] ——, "Weighted sum power maximization for intelligent reflecting surface aided SWIPT," *IEEE Wireless Commun. Lett.*, vol. 9, no. 5, pp. 586–590, May 2020.

[19] K. Ntontin, J. Song, and M. D. Renzo, "Multi-antenna relaying and reconfigurable intelligent surfaces: End-to-end SNR and achievable rate," *Arxiv*, vol. 1908.07967v2, pp. 1–1, Aug. 2019.

[20] X. Yu, D. Xu, and R. Schober, "MISO wireless communication systems via intelligent reflecting surfaces," in *2019 IEEE/CIC International Conference on Communications in China (ICCC)*, 2019, pp. 735–740.

[21] E. Basar, "Reconfigurable intelligent surface-based index modulation: A new beyond MIMO paradigm for 6G," *IEEE Trans. Commun.*, vol. 68, no. 5, pp. 3187–3196, May 2020.

[22] Y. Han, W. Tang, S. Jin, C. Wen, and X. Ma, "Large intelligent surface-assisted wireless communication exploiting statistical CSI," *IEEE Trans. Veh. Tech.*, vol. 68, no. 8, pp. 8238–8242, Aug. 2019.

[23] N. Bhargav, C. R. N. da Silva, Y. J. Chun, È. J. Leonardo, S. L. Cotton, and M. D. Yacoub, "On the product of two κ-μ random variables and its application to double and composite fading channels," *IEEE Transactions on Wireless Communications*, vol. 17, no. 4, pp. 2457–2470, 2018.

[24] M. Jung, W. Saad, Y. Jang, G. Kong, and S. Choi, "Performance analysis of large intelligent surfaces (LISs): Asymptotic data rate and channel hardening effects," *IEEE Transactions on Wireless Communications*, vol. 19, no. 3, pp. 2052–2065, Mar. 2020.

[25] B. Zheng, Q. Wu, and R. Zhang, "Intelligent reflecting surface-assisted multiple access with user pairing: NOMA or OMA?" *IEEE Commun. Lett.*, vol. 24, no. 4, pp. 753–757, Apr. 2020.

[26] T. Hou, Y. Liu, Z. Song, X. Sun, Y. Chen, and L. Hanzo, "Reconfigurable intelligent surface aided NOMA networks," *IEEE J. Sel. Areas Commun.*, vol. 38, no. 11, pp. 2575–2588, Nov. 2020.

[27] S. Zhang and R. Zhang, "Intelligent reflecting surface aided multi-user communication: Capacity region and deployment strategy," *IEEE Trans. Commun.*, vol. 69, no. 9, pp. 5790–5806, Sept. 2021.

[28] L. Dai, B. Wang, M. Wang, X. Yang, J. Tan, S. Bi, S. Xu, F. Yang, Z. Chen, M. D. Renzo, C. Chae, and L. Hanzo, "Reconfigurable intelligent surface-based wireless communications: Antenna design, prototyping, and experimental results," *IEEE Access*, vol. 8, pp. 45 913–45 923, 2020.

[29] B. Di, H. Zhang, L. Li, L. Song, Y. Li, and Z. Han, "Practical hybrid beamforming with finite-resolution phase shifters for reconfigurable intelligent surface based multi-user communications," *IEEE Transactions on Vehicular Technology*, vol. 69, no. 4565-4570, pp. 1–1, Apr. 2020.

[30] H. Zhang, B. Di, L. Song, and Z. Han, "Reconfigurable intelligent surfaces assisted communications with limited phase shifts: How many phase shifts are enough?" *IEEE Transactions on Vehicular Technology*, vol. 69, no. 4, pp. 4498–4502, Apr. 2020.

[31] Q. Wu and R. Zhang, "Beamforming optimization for intelligent reflecting surface with discrete phase shifts," in *ICASSP 2019 - 2019 IEEE International Conference on Acoustics, Speech and Signal Processing (ICASSP)*, 2019, pp. 7830–7833.

[32] Q. Nadeem, A. Kammoun, A. Chaaban, M. Debbah, and M. Alouini, "Large intelligent surface assisted MIMO communications," *Arxiv*, vol. 1903.08127v1, Mar. 2019.

[33] C. Huang, G. C. Alexandropoulos, A. Zappone, M. Debbah, and C. Yuen, "Energy efficient multi-user MISO communication using low resolution large intelligent surfaces," in *2018 IEEE GLOBECOM Workshops (GC Wkshps)*, Dec. 2018, pp. 1–6.

[34] C. Huang, A. Zappone, G. C. Alexandropoulos, M. Debbah, and C. Yuen, "Reconfigurable intelligent surfaces for energy efficiency in wireless communication," *IEEE Trans. Wireless Commun.*, vol. 18, no. 8, pp. 4157–4170, Aug. 2019.

[35] J. Zhu, Y. Huang, J. Wang, K. Navaie, and Z. Ding, "Power efficient IRS-assisted NOMA," *IEEE Transactions on Communications*, vol. 68, no. 2, pp. 900–913, Feb. 2021.

[36] C. Psomas and I. Krikidis, "Low-complexity random rotation-based schemes for intelligent reflecting surfaces," *IEEE Transactions on Wireless Communications*, vol. Accepted to appear, 2021.

[37] L. Zhang, L. Yan, B. Lin, H. Ding, Y. Fang, and X. Fang, "Augmenting transmission environments for better communications: Tunable reflector assisted mmWave WLANs," *IEEE Trans. Veh. Tech.*, vol. 69, no. 7, pp. 7416–7428, Jul. 2020.

[38] Z. Wang, L. Liu, and S. Cui, "Channel estimation for intelligent reflecting surface assisted multiuser communications: Framework, algorithms, and analysis," *IEEE Transactions on Wireless Communications*, vol. 19, no. 10, pp. 6607–6620, Oct. 2020.

[39] Z. Zhou, N. Ge, Z. Wang, and L. Hanzo, "Joint transmit precoding and reconfigurable intelligent surface phase adjustment: A decomposition-aided channel estimation approach," *IEEE Transactions on Communications*, vol. 69, no. 2, pp. 1228–1243, Feb. 2021.

[40] Y. Han, W. Tang, S. Jin, C. Wen, and X. Ma, "Large intelligent surface-assisted wireless communication exploiting statistical CSI," *IEEE Transactions on Vehicular Technology*, vol. 68, no. 8, pp. 8238–8242, 2019.

[41] H. Jiang, C. Ruan, Z. Zhang, J. Dang, L. Wu, M. Mukherjee, and D. B. d. Costa, "A general wideband non-stationary stochastic channel model for intelligent reflecting surface-assisted mimo communications," *IEEE Transactions on Wireless Communications*, vol. 20, no. 8, pp. 5314–5328, Aug. 2021.

[42] Y. Sun, C.-X. Wang, J. Huang, and J. Wang, "A 3D non-stationary channel model for 6G wireless systems employing intelligent reflecting surface," in *2020 International Conference on Wireless Communications and Signal Processing (WCSP)*, 2020, pp. 19–25.

[43] D. Stoyan, W. Kendall, and J. Mecke, *Stochastic Geometry and Its Applications*. John Wiley and Sons, 2nd Ed, 1996.

[44] M. Haenggi, *Stochastic Geometry for Wireless Networks*. Cambridge, U.K.: Cambridge Univ. Press, 2012.

[45] M. Haenggi, J. G. Andrews, F. Baccelli, O. Dousse, and M. Franceschetti, "Stochastic geometry and random graphs for the analysis and design of wireless networks," *IEEE J. Sel. Topics Signal Process*, vol. 27, no. 7, pp. 1029–1046, Sep. 2009.

[46] J. G. Andrews, F. Baccelli, and R. K. Ganti, "A tractable approach to coverage and rate in cellular networks," *IEEE Trans. Commun.*, vol. 59, no. 11, pp. 3122–3134, Nov. 2011.

[47] M. A. Kishk and M.-S. Alouini, "Exploiting randomly located blockages for large-scale deployment of intelligent surfaces," *IEEE Journal on Selected Areas in Communications*, vol. 39, no. 4, pp. 1043–1056, Apr. 2021.

[48] J. Lyu and R. Zhang, "Hybrid active/passive wireless network aided by intelligent reflecting surface: System modeling and performance analysis," *IEEE Transactions on Wireless Communications*, pp. 1–1, Accepted to appear 2021.

[49] H. Liu, X. Yuan, and Y. Jun, "Reconfigurable intelligent surfaces aided multi-cell NOMA networks: A stochastic geometry model," *arXiv*, vol. 2008.08457v1, Aug. 2020.

[50] I. S. Gradshteyn and I. M. Ryzhik, *Table of Integrals, Series and Products*. New York: Academic Press, 6th Ed, 2000.

[51] T. Hou, Y. Liu, Z. Song, X. Sun, and Y. Chen, "Exploiting NOMA for UAV communications in large-scale cellular networks," *IEEE Trans. Commun.*, vol. 67, no. 10, pp. 6897–6911, Oct. 2019.

[52] Z. Ding, F. Adachi, and H. V. Poor, "The application of MIMO to non-orthogonal multiple access," *IEEE Trans. Wireless Commun.*, vol. 15, no. 1, pp. 537–552, Jan. 2016.

[53] F. P. Fontn and P. M. Espieira, *Modelling the wireless propagation channel: A simulation approach with MATLAB*. John Wiley and Sons, 2008.

[54] H. Liu, X. Yuan, and Y. Jun, "Matrix-calibration-based cascaded channel estimation for reconfigurable intelligent surface assisted multiuser MIMO," *ArXiv*, vol. 1912.09025, Dec. 2019.

[55] B. Zheng and R. Zhang, "IRS meets relaying: Joint resource allocation and passive beamforming optimization," *IEEE Wireless Commun. Lett.*, vol. 10, no. 9, pp. 2080–2084, Sept. 2021.

[56] Q. Wu and R. Zhang, "Intelligent reflecting surface enhanced wireless network via joint active and passive beamforming," *IEEE Transactions on Wireless Communications*, vol. 18, no. 11, pp. 5394–5409, Nov. 2019.

[57] Y. Zhang, F. Gao, L. Fan, X. Lei, and G. K. Karagiannidis, "Backscatter communications over correlated Nakagami-m fading channels," *IEEE Trans. Commun.*, vol. 67, no. 2, pp. 1693–1704, Feb. 2019.

[58] L. N. Ribeiro, S. Schwarz, M. Rupp, and A. L. F. de Almeida, "Energy efficiency of mmWave massive MIMO precoding with low-resolution DACs," *IEEE J. Sel. Topics Signal Process*, vol. 12, no. 2, pp. 298–312, May 2018.

[59] J. N. Laneman, D. N. C. Tse, and G. W. Wornell, "Cooperative diversity in wireless networks: Efficient protocols and outage behavior," *IEEE Trans. Information Theory*, vol. 50, no. 12, pp. 3062–3080, Dec. 2004.